The dynamics of NH_4^+ in the NH_4MF_3 perovskites: I. A quasielastic neutron scattering study

1994 J. Phys.: Condens. Matter 6 8449

(http://iopscience.iop.org/0953-8984/6/41/008)

J. Phys.: Condens. Matter 6 (1994) 8449–8468. Printed in the UK

The dynamics of NH_4^+ in the NH_4MF_3 perovskites: I. A quasielastic neutron scattering study

J Rubín†, J Bartolomé†, M Anne‡, G J Kearley§ and A Magerl§

† Instituto de Ciencia de Materiales de Aragón, CSIC—Universidad de Zaragoza, 50009 Zaragoza, Spain

‡ Laboratoire de Cristallographie, CNRS, 38043 Grenoble, France

§ Institut Laue–Langevin, 38043 Grenoble, France

Received 10 November 1993, in final form 31 May 1994

Abstract. Quasielastic neutron scattering experiments have been carried out to study the thermally activated rotational process of the NH_4^+ ion in the perovskite family NH_4MF_3 (M = Mg, Zn, Mn and Cd). The activation energies of this process in the high- and low-temperature structural phases have been obtained, and range from 44.8 meV for NH_4MgF_3 to 128 meV for NH_4CdF_3 in the high-temperature phase, and from 75 meV for NH_4ZnF_3 to 246 meV for NH_4CdF_3 in the low-temperature phase. Geometric models for the orientations of the NH_4^+ ion occupied during the rotational process are proposed in both phases. In the high-temperature phase, the dominant rotations are around twofold axes. A preferential axis, determined by the orientations of the ion in the crystal, shows the greatest jump rate. In the low-temperature phase the rotational disorder persists through two energetically non-equivalent orientations.

1. Introduction

The experimental study of the dynamics of molecular groups in solids is fundamental for understanding of the interactions between those molecules and their lattice environment. The molecule can be an electrically neutral one (e.g. NH_3 or CH_4) or an ion (e.g. NH_4^+), which determines the dominant interaction. In an ionic solid the dominant interaction usually originates from the localized charge distributions on the ions and can be approximated by point charges.

Compounds with NH_4^+ ionic molecular groups are suitable for the study of a three-dimensional rotator in ionic solids (Hüller and Press 1978), including the symmetry properties of its dynamics. This can be probed in the different phenomena that can be measured: hindered rotations (librations) of the molecule in a potential well, classical rotational jumps over the potential barriers, and tunnelling. Each kind of motion has a different energy range and can be measured in different ways.

The intensity of the interaction between the NH_4^+ ion and its environment is high for the NH_4X (X = F, Cl) halides, with activation energies for the jump process over 175 meV (Woessner and Snowdon 1967). In contrast, $(NH_4)_2MCl_6$ compounds show low barriers (usually below 60 meV) (Svare *et al* 1978, Kearley and Oxton 1983), which has been interpreted as due to an important repulsive component in the total interaction, originating from overlap of H and halide orbitals (Hüller and Raich 1979). These conclusions have been derived from NMR and neutron scattering experiments, which yielded their activation energies and librational energies; these are well established for the series of compounds mentioned above (Bonori and Terenzi 1974, Prager *et al* 1977, Svare *et al* 1978).

0953-8984/94/418449+20$19.50

The fluoroperovskites NH_4MF_3 (M = Mg, Zn, Mn, Cd) constitute another family of ammonium compounds with particular characteristics. There is contradictory information about the dynamics of the NH_4^+ rotator, which has not allowed an unambiguous situation of this family in the above description. These compounds are cubic at high temperature, and undergo a structural phase transition to a lower-symmetry phase on cooling.

When cooled, the low-temperature structure is orthorhombic, as has been determined by x-ray diffraction in NH_4CdF_3 (Le Bail *et al* 1990), NH_4ZnF_3 (Fayos and Tornero 1993) and NH_4MnF_3 (Laguna *et al* 1993). In the latter, this result was checked with Raman spectroscopy. For NH_4MgF_3, the structure is at least tetragonal at low temperature, and only the tetragonal cell parameters have been measured (Palacios *et al* 1986). The structural transition affects the NH_4^+ ion, as is nicely shown in the calorimetric measurements by a high peak at T_c with an entropy content over 1 R (Bartolomé *et al* 1977, Burriel *et al* 1981, Palacios *et al* 1984, 1986). This means that the number of rotational degrees of freedom of the NH_4^+ group in the lattice has decreased, as a consequence of the lower crystal symmetry of the low-temperature phase (Bartolomé *et al* 1977).

The microscopic description of the rotational jumps of the NH_4^+ groups in ammonium compounds is not abundant (Kim *et al* 1970, Dahlborg *et al* 1970, Livingston *et al* 1974, Töpler *et al* 1978, Steenbergen *et al* 1979, Grimm *et al* 1989, Lucazeau *et al* 1990). In most cases, only the activation energy of the thermally activated jumps was obtained. In the perovskites, only for NH_4ZnF_3 in the cubic phase is there a study with quasielastic neutron scattering (QNS) (Steenbergen *et al* 1979), where the activation energy was obtained, and it was concluded that the most frequent jump of the ammonium ion corresponded to 90° rotations around a single axis. Some of the activation energies in both structural phases are known from NMR experiments (Brom and Bartolomé 1981, Raaen *et al* 1982, Palacios *et al* 1984, 1989), though with the gap of the Mn compound, since the Mn paramagnetic ion avoids the measurement of the relaxation time of the NH_4^+ jump process. However, the existing data in the low-temperature phase show that E_a increases for increasing cell parameters in either phase, which is contrary to expectation for dominant electrostatic interactions. In the high-temperature phase, the same trend seems to hold, but there are not enough data for an unambiguous conclusion. On the other hand, the activation energy in the low-temperature phase is larger than that in the high-temperature phase, and the relaxation time shows a step at the transition temperature. From NMR measurements there are also estimations of the librational energies in the distorted phase (Palacios *et al* 1989), but they seem to be too small (13 meV for Mg and 17 meV for Zn compounds) or too large (95 meV for the Cd compound) for fluorides (the librational energy of NH_4^+ in NH_4F is 69 meV (Leung *et al* 1972)).

The study on the ammonium fluoroperovskites has also been extended to NH_4MnCl_3 (Burriel *et al* 1981, Piqué *et al* 1990). This has a cubic high-temperature phase and an orthorhombic phase below 255 K (Agulló-Rueda *et al* 1987). Since the halide is Cl and the cell parameters are larger than those of the fluorides, NH_4MnCl_3 was proposed as a candidate for quasi-free rotations of the NH_4^+ group in a solid. QNS experiments (Rubín *et al* 1989) have shown that the NH_4^+ rotator is not free. The activation energies in the two phases are similar and around 60.3 meV, and the jump rates also show a step at T_c. At the transition temperature (255 K), the librational levels (estimated from the quasielastic jump rates) must be not negligibly populated, and therefore the activation energies obtained from the quasielastic broadenings do not represent jumps from the rotational ground state. This may produce the similarity in the experimental activation energies in the two structural phases.

That is the starting point of our investigations on the dynamics of the NH_4^+ group in

fluoroperovskites. This work is separated in two papers (from now on referred to as I and II), which are dedicated to the rotational process and the librational motions respectively. In the first paper, the rotational jumps over the potential barriers are studied by QNS, which allows for a spatial resolution of this process, and direct geometry time of flight (TOF) spectrometers are preferably used. On the other hand, the librational energies are sought in the inelastic neutron scattering (INS) spectra from a crystal analyser spectrometer with inverted geometry.

In this paper, the experimental conditions and the data reduction are indicated in sections 2 and 3, and the results are introduced. In section 4 we describe the models for the rotations that the NH_4^+ ion can perform, while section 5 is devoted to a discussion of these models and the rotational process.

2. Experimental measurements and data treatment

QNS spectra of the perovskites NH_4MgF_3, NH_4MnF_3 and NH_4CdF_3 were obtained in the TOF spectrometers IN5 and IN6 at the Institut Laue–Langevin in Grenoble, while for NH_4ZnF_3 in the low-temperature phase the backscattering spectrometer IN10 was used. The instruments and technical conditions of the experiments for each compound are summarized in table 1. In the experiments on IN5 and IN6, the powder samples were placed in flat containers, which were oriented with the line perpendicular to the plane of the container forming an angle of 45° with the incident beam, and only the scattered intensity through the sample was measured. This orientation allows measurements at scattering angles around 45° with a small sample thickness and reasonable values of the momentum transfer, but the highest values of the momentum transfer (detectors at angles of more than 100°) correspond to long paths in the sample. The detectors were grouped in order to improve counting statistics.

In the case of the Mn compound, two sets of experiments with incident neutron beams of different wavelengths, λ_0, were performed. This allows for different resolution widths of the elastic peak: $\Delta E \simeq 115$ μeV for $\lambda_0 = 4.9$ Å, and $\Delta E \simeq 320$ μeV for $\lambda_0 = 3.5$ Å. Further, the energy window is expanded with decreasing incident wavelength. Resolution width and energy window depend on incident wavelength in opposite ways. Thus, the use of two sets of measurements with different incident λ_0 is intended for a more extensive study of the quasielastic broadening due to the relaxation process of rotation.

The raw data were calibrated with a separate measuring run of an incoherent scatterer V plate. The experimental background was measured with the empty Al container at room temperature. This background includes the noise and container contributions to the sample raw data. The scattering from the non-hydrogeneous elements of the samples was not taken into account, since their scattering can be considered to be negligible as a consequence of the much larger scattering cross section of H. Using measured transmission factors of the samples (table 1) for the same experimental set-up, the corrections for absorption and self-shielding were performed with standard computer programs (Ghosh 1985). The resultant spectra give the scattering function, $S(\phi, \omega)$, where ϕ is the scattering angle and $\hbar\omega$ is the energy transfer. Finally, the corrected experimental spectra were fitted to a sum of a delta function and a Lorentzian, including the detailed balance factor, convoluted with the experimental resolution (the V run). A flat background (in TOF) was also included in the fit. In this way the quasielastic widths and the relative intensities of the elastic and quasielastic components were obtained.

Though, in general, the scattering function for the rotational jumps of a molecule in a solid is composed of a delta function and several Lorentzians, reasonable fits could only

Table 1. Instruments used and experimental conditions of the neutron scattering experiments in this work (Blank and Maier 1988). λ_0 is the wavelength of the incident neutrons, Q is the momentum transfer range for elastic scattering, ΔE is the full width at half maximum of the resolution spectrum, t is the transmission factor. IN10 is a spectrometer of inverted geometry, and the corresponding λ_0 is the wavelength of the scattered neutrons determined by the analyser.

Compound	$T < T_c$	$T > T_c$
NH_4MgF_3	—	IN5 $\lambda_0 = 4.9$ Å $\Delta E \simeq 115$ μeV $0 < Q < 2.34$ Å^{-1} $t = 0.88$
NH_4ZnF_3	IN10 $\lambda_0 = 6.27$ Å $\Delta E \simeq 0.3$ μeV $0 < Q < 2.34$ Å^{-1}	Steenbergen *et al* 1979
NH_4MnF_3	IN5 $\lambda_0 = 4.9$ Å $\Delta E \simeq 115$ μeV $0 < Q < 2.34$ Å^{-1} $t = 0.88$	IN5 $\lambda_0 = 4.9$ Å $\Delta E \simeq 115$ μeV $0 < Q < 2.34$ Å^{-1} $t = 0.88$ $\lambda_0 = 3.5$ Å $\Delta E \simeq 320$ μeV $0 < Q < 3.25$ Å^{-1} $t = 0.88$
NH_4CdF_3	IN6 $\lambda_0 = 5.1$ Å $\Delta E \simeq 100$ μeV $0 < Q < 2$ Å^{-1} $t = 0.073$	IN6 $\lambda_0 = 5.1$ Å $\Delta E \simeq 100$ μeV $0 < Q < 2$ Å^{-1} $t = 0.073$

be obtained using a sum of a delta function and a single Lorentzian for our spectra. This may affect the values of the elastic intensity when actually there are several Lorentzian components. These effects will be discussed in subsection 4.1. Therefore, the elastic incoherent structure factor (EISF), which contains the geometric information of the jumps, was calculated in the following way: first, the theoretical scattering function $S(Q, \omega)$ was convoluted with the experimental resolution function $R(Q, \omega)$

$$S_{\mathrm{exp}}(Q, \omega) = \int S(Q, \omega')R(Q, \omega - \omega')\,\mathrm{d}\omega'.$$

We made the approximation $S(Q, \omega) \simeq S(\phi, \omega)$ and the scattering momentum transfer of the energy spectrum $S(Q, \omega)$ was taken as $Q_0 \simeq Q(\phi, \omega = 0)$. The function used for the fits was

$$S(Q, \omega) = \mathrm{e}^{-\hbar\omega/2kT}[I_\delta(Q)\delta(\omega) + I_{\mathrm{L}}(Q)(1/\pi)(\Gamma/2)/[(\Gamma/2)^2 + (\omega)^2]] + B$$

where B is a constant background in time of flight, $I_\delta(Q)$ and $I_{\mathrm{L}}(Q)$ are the intensities of the delta and Lorentzian functions, respectively, and Γ is the full width at half maximum of the Lorentzian. The exponential is the detailed balance factor. Then, the EISF is calculated

as

$$\text{EISF} = \frac{I_\delta(Q)}{I_\delta(Q) + I_L(Q)}$$

where $I_\delta(Q)$ and $I_L(Q)$ both contain the Debye–Waller factor due to the internal and torsional motions of the NH_4^+ ion. This factor cancels in the calculation of the EISF.

3. Data analysis

3.1. Elastic incoherent structure factor

The plot of the EISF versus Q of the compounds NH_4MF_3 (M=Mg, Mn and Cd) is presented in figure 1. We immediately note that the EISF is temperature dependent. In NH_4MnF_3 and NH_4MgF_3 in the cubic phase (figure 1(*b*) and (*c*)), the experimental EISF tends smoothly towards the same values when the transition temperature is reached. In contrast, for NH_4CdF_3 in the cubic phase ($T > T_c = 331$ K), the EISF is temperature independent.

Multiple-scattering effects show up at small scattering angles, as can be seen in the EISFs in figure 1, which should tend to one as Q tends to zero. However, for nuclear species with large cross section for neutron absorption, multiple scattering is always negligible, which is verified by NH_4CdF_3. Therefore, in the case of NH_4MgF_3 and NH_4MnF_3 the values of the EISF and widths for low scattering angles cannot be used without a previous treatment of the multiple scattering. In fact, for Q tending to zero, the EISF tends to 0.82 in the most unfavourable case (the theotetical value is unity). This is not a very low value as compared with other experiments on other compounds (e.g., $\text{EISF}(Q = 0) = 0.72$ for a transmission factor $T = 0.8$ in triethylenediamine, Bée 1988).

At the highest scattering angles in the experiments, multiple-scattering effects can also be non-negligible. However, the EISF of NH_4MnF_3 at a given temperature (e.g. 190 and 220 K, figure 1(*e*)) and different incident neutron wavelength (3.5 and 4.9 Å) are the same within experimental error. Therefore, the values of the EISF at highest Q values (highest scattering angles and corresponding sample thickness) and $\lambda_0 = 4.9$ Å, which should be affected by multiple scattering, do not show any significant difference from those with similar Q values (~ 2.4 Å^{-1}) but lower scattering angles and sample thickness corresponding to the experiment with a shorter wavelength (3.5 Å). As a consequence, the correction for multiple scattering has not been attempted and only the values of Q where multiple scattering can be considered negligible for our purposes have been used. This is not important to account for differences in the EISF, since the theoretical EISF for the different models does not show any substantial difference below $Q = 1$ Å^{-1}.

3.2. Activation energies

Figure 2 shows the quasielastic half widths versus $1/T$, which were used to calculate the activation energies of the rotational process assuming an Arrhenius law: $\Gamma = \Gamma_0 e^{-E_a/kT}$. Only values of the widths for $Q > 1$ Å^{-1} were used, in order to minimize multiple-scattering effects. The values of E_a obtained with QNS (table 2) compare reasonably well with those from NMR experiments (Brom and Bartolomé 1981, Raaen *et al* 1982, Palacios *et al* 1984, 1989) and extend the conclusions on the trends of the activation energies in this family of compounds (Palacios *et al* 1989): (i) the increase of E_a with the cell parameters is also verified in the high-temperature phase, and (ii) the trend in the low-temperature phase, as indicated by the Cd compound, is also fulfilled by the intermediate compound NH_4MnF_3.

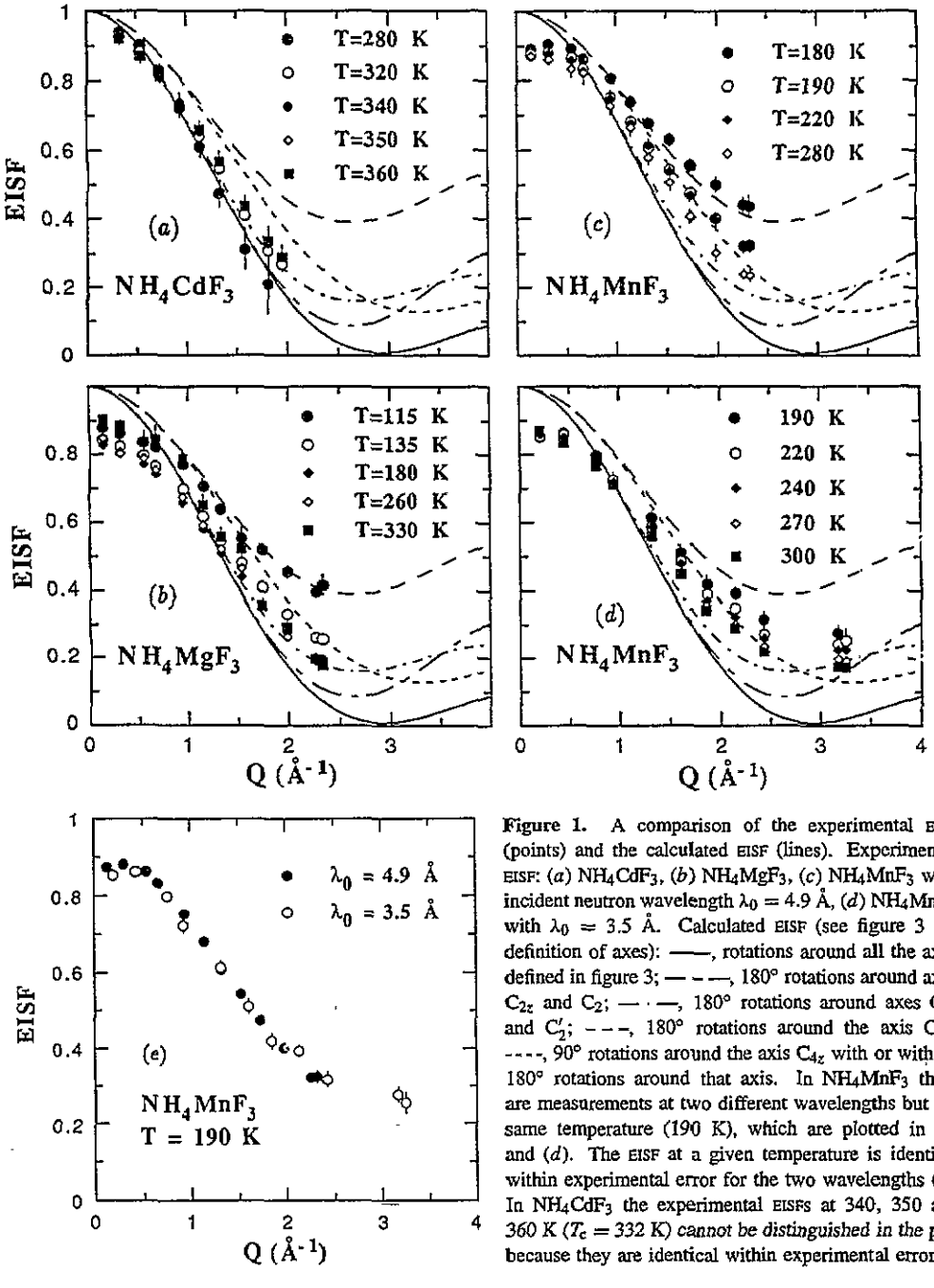

Figure 1. A comparison of the experimental EISF (points) and the calculated EISF (lines). Experimental EISF: (*a*) NH_4CdF_3, (*b*) NH_4MgF_3, (*c*) NH_4MnF_3 with incident neutron wavelength $\lambda_0 = 4.9$ Å, (*d*) NH_4MnF_3 with $\lambda_0 = 3.5$ Å. Calculated EISF (see figure 3 for definition of axes): ——, rotations around all the axes defined in figure 3; — – —, 180° rotations around axes C_{2z} and C_2; — · —, 180° rotations around axes C_{2z} and C_2'; – – –, 180° rotations around the axis C_{2z}; ----, 90° rotations around the axis C_{4z} with or without 180° rotations around that axis. In NH_4MnF_3 there are measurements at two different wavelengths but the same temperature (190 K), which are plotted in (*c*) and (*d*). The EISF at a given temperature is identical within experimental error for the two wavelengths (*e*). In NH_4CdF_3 the experimental EISFs at 340, 350 and 360 K ($T_c = 332$ K) cannot be distinguished in the plot because they are identical within experimental error.

In the case of the Cd compound in the low-temperature phase, there are measurements at only two temperatures. An activation energy of 246 meV can be estimated, which is much larger than the value obtained by NMR (Palacios *et al* 1989), 168 meV. The large value from the neutron experiments is probably due to resolution problems, since the broadening at 280 K is narrower than the resolution width (100 μeV), and the quasielastic peak can

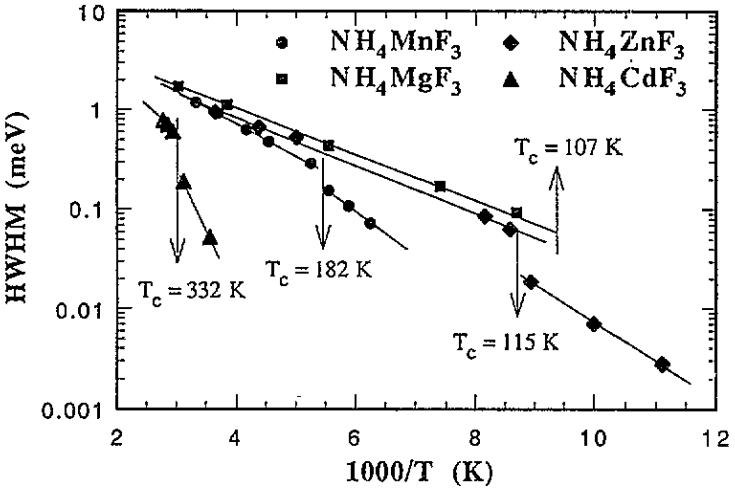

Figure 2. An Arrhenius plot of the quasielastic half widths at half maximum (HWHM) versus the reciprocal of the temperature.

Table 2. Activation energies of the rotational process in both structural phases. Numbers in bold are those obtained in this work. References of other data: [1] Palacios *et al* (1986); [2] Helmholdt *et al* (1980); [3] Palacios *et al* (1989); [4] Steenbergen *et al* (1979); [5] Brom and Bartolomé (1981); [6] Laguna *et al* (1993); [7] Le Bail *et al* (1990). The orthorhombic cell parameters a, b and c are related to the pseudocubic cell parameters a_{pc}, b_{pc} and c_{pc} (distorsion of the high-temperature cubic unit cell) by $a \simeq \sqrt{2}a_{pc}$, $b \simeq 2b_{pc}$, $c \simeq \sqrt{2}c_{pc}$.

	NH_4MgF_3	NH_4ZnF_3	NH_4MnF_3	NH_4CdF_3
$T > T_c$				
a (Å)	4.056[1]	4.118[2]	4.242[2]	4.390[3]
E_a (meV) [QNS]	**44.8 ± 0.9**	50.0 ± 1.3[4]	**62.9 ± 1.7**	**128 ± 26**
τ_0 (ps)	**0.082**	0.052	**0.049**	**0.014**
E_a (meV) [RMN]	38.8 ± 4.3[3]	58.6 ± 1.7[5]	—	—
τ_0 (ps)	—	0.04	—	—
T_c (K)	107	115	182	332
$T < T_c$				
a (Å)	4.026[1]	4.0808[2]	5.952[6]	6.1791[7]
b (Å)	—	—	8.543	8.8786
c (Å)	4.080	4.150	5.949	6.1655
E_a (meV) [QNS]	—	**75 ± 6**	**93 ± 7**	**246**
τ_0 (ps)	—	**0.016**	**0.011**	**0.0005**
E_a (meV) [RMN]	65.5 ± 4.3[3]	71.1 ± 1.7[3,5]	—	168.1 ± 4.3[3]
τ_0 (ps)	0.2	0.1	—	0.024

hardly be separated from the elastic peak. This can also be observed in the low values of the EISF at 280 K (figure 1(a)): the EISF is underestimated and its intensity has passed to the central part of the quasielastic component, which compels it to be narrow. The NMR value for E_a is therefore considered more reliable.

Since the general mode of rotations may give rise to more than one Lorentzian function

and only one is fitted (the most intense one), these activation energies should be considered as an average for the possible types of jump on different axes of rotation or for those types that take part in the width of the fitted Lorentzian (*vide infra*).

4. Models for rotations of the NH_4^+ ion

In order to interpret the experimental EISF (figure 1) we propose geometric models for the rotations of the NH_4^+ ion in the high and low-temperature phases of the NH_4MF_3 family.

4.1. Models of rotation in the high-temperature phase

Following the formalism developed by Thibaudier and Volino (Thibaudier and Volino 1973, 1975, Bée 1988), one starts from a set of proper rotations that constitute a group G. All rotations, R, will be regarded as instantaneous, and those belonging to the same class, μ, will be assigned the same jump rate τ_μ^{-1}. Under these assumptions, the intermediate function, $I(Q,t)$ can be written

$$I_{\text{inc}}(Q,t) = \sum_\alpha A_\alpha(Q)\exp\{-t/\tau_\alpha\}$$

where $A_\alpha(Q)$ is the incoherent structure factor corresponding to the irreducible representation α of the point group G. $A_\alpha(Q)$ and τ_α are given by

$$A_\alpha(Q) = \frac{\chi_\alpha^E}{g}\sum_\mu\sum_{R_\mu}\exp\{\mathbf{i}Q\cdot(r - R_\mu r)\}\chi_\alpha^\mu$$

$$\frac{1}{\tau_\alpha} = \sum_\mu \frac{n_\mu}{\tau_\mu}\left(1 - \frac{\chi_\alpha^\mu}{\chi_\alpha^E}\right)$$

where the summation is over the classes μ, χ_α^μ are the characters of G, and E is the identity of G. For the totally symmetric representation, $\alpha = A$, it is obvious that $\tau_A^{-1} = 0$. For a powder sample

$$A_\alpha(Q) = \frac{\chi_\alpha^E}{g}\sum_\mu\sum_{R_\mu}\chi_\alpha^\mu j_0(Q|r - R_\mu r|).$$

Finally, the scattering function can be written in the following way

$$S_{\text{inc}}(Q,\omega) = \frac{1}{2\pi}\int_{-\infty}^{\infty} I(Q,t)e^{i\omega t}dt = A_A(Q)\delta(\omega) + \sum_{\alpha\neq A} A_\alpha(Q)\frac{1}{\pi}\frac{\lambda_\alpha}{\omega^2 + \lambda_\alpha^2}$$

where $\lambda_\alpha = \tau_\alpha^{-1}$ for $\alpha \neq A$ and $A_A(Q)$ is the EISF.

In the most general model, all the axes of rotation of the crystal and the molecule must be taken into account. In figure 3 these axes are defined on the cubic cage of the crystal and the cube inscribing the NH_4^+ tetrahedron. Such a general model will give an EISF that rapidly decreases to zero as Q increases. Restrained models can be used by setting to zero the jump rates of certain rotations around certain axes, and their structure factors should now be included in the EISF. In this way, the non-resolved quasielastic components that

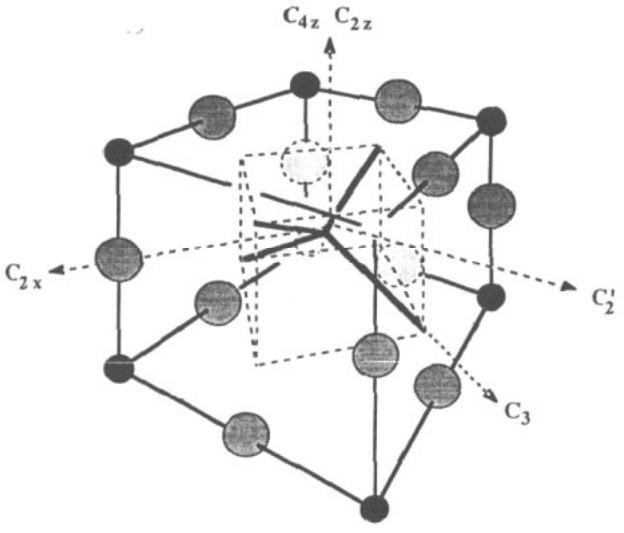

Figure 3. Axes of rotation defined on the cube inscribing the tetrahedron in its equlibrium orientation.

Table 3. Structure factors and relaxation times for rotations around the axes of the cube inscribing the NH_4^+ tetrahedron.

$G = D_4$ Irreducible Representations $= \{A_1, A_2, B_1, B_2, E\}$
$\tau_{A_1}^{-1} = 0$
$\tau_{A_2}^{-1} = 4(\tau_{C_{2x}}^{-1} + \tau_{C_2'}^{-1})$
$\tau_{B_1}^{-1} = 4(\tau_{C_{4z}}^{-1} + \tau_{C_2'}^{-1})$
$\tau_{B_2}^{-1} = 4(\tau_{C_{4z}}^{-1} + \tau_{C_{2x}}^{-1})$
$\tau_E^{-1} = 2(\tau_{C_{2z}}^{-1} + \tau_{C_{4z}}^{-1} + \tau_{C_{2x}}^{-1} + \tau_{C_2'}^{-1})$
$A_{A_1}(Q) = \frac{1}{8}[1 + 3j_0(\sqrt{2}aQ) + 3j_0(aQ) + j_0(\sqrt{3}aQ)]$
$A_{A_2}(Q) = \frac{1}{8}[1 - j_0(\sqrt{2}aQ) + j_0(aQ) - j_0(\sqrt{3}aQ)]$
$A_{B_1}(Q) = \frac{1}{8}[1 + 3j_0(\sqrt{2}aQ) - 3j_0(aQ) - j_0(\sqrt{3}aQ)]$
$A_{B_2}(Q) = \frac{1}{8}[1 - j_0(\sqrt{2}aQ) - j_0(aQ) + j_0(\sqrt{3}aQ)]$
$A_E(Q) = \frac{1}{8}[4 - 4j_0(\sqrt{2}aQ)]$
$a = 2\frac{d_{N-H}}{\sqrt{3}}$

contribute to the experimental EISF can be simulated. The types of jump with rates set to zero actually have too long relaxation times to be resolved in the present experiment.

The theoretical EISFs of several models of rotations of the NH_4^+ group in the cubic perovskite cage formed by the nearest 12 fluorine and eight metal ions were calculated (figure 1 and table 3). Since the experimental EISF falls between two of the calculated curves, we shall first analyse the two models that explain the two limiting bounds of the experimental EISF, and, in a second step, an interpretation for the temperature dependence of the EISF will be proposed.

(i) The lower bound corresponds to the EISF as temperature increases and is attained above room temperature for the Zn and Mn compounds, while for NH_4CdF_3 this bound is already reached at the transition temperature ($T_c = 332$ K) and no further temperature dependence can be observed. The corresponding geometric model only considers rotations of 180° around three perpendicular twofold axes of the crystal cubic cage of the NH_4^+. One of these axes, C_{2z}, coincides with an NH_4^+ twofold axis, and is also a crystal fourfold axis (figure 3). This particular axis is defined by the orientation of the NH_4^+ in the crystal. The two other axes are C_2' axes of the cube inscribing the tetrahedron perpendicular to the C_{2z} axis, but they are not symmetry axes of the tetrahedron. This model allows for only two orientations of the molecule from the six possible ones. The 180° jumps around the C_{2z} axis leave the NH_4^+ invariant, while the change of orientation is produced by rotations around the C_2' axes. The other four orientations may be reached through other types of rotation with much smaller jump rates and would not be observable in the present experiment. For this model, the scattering function is

$$S(Q,\omega) = [A_{A_1}(Q) + A_{B_2}(Q)]\delta(\omega) + [A_{A_2}(Q) + A_{B_1}(Q)]L(\omega,\lambda_1) + A_E(Q)L(\omega,\lambda_2)$$

$$\lambda_1 = 4\tau_{C_2'}^{-1} \qquad \lambda_2 = 2(\tau_{C_{2z}}^{-1} + \tau_{C_2'}^{-1}). \tag{1}$$

(ii) Now the upper-bound model is considered, which will correspond to temperatures near the transition ($T_c = 182$ K for NH_4MnF_3 and $T_c = 107$ K for NH_4MgF_3). In this model only 180° jumps around the unique axis C_{2z} are taken into account. The corresponding scattering function is

$$S(Q,\omega) = [A_{A_1}(Q) + A_{A_2}(Q) + A_{B_2}(Q) + A_{B_1}(Q)]\delta(\omega) + A_E(Q)L(\omega,\lambda) \qquad \lambda = 2\tau_{C_{2z}}^{-1}.$$

4.2. The temperature dependence of the EISF in the high-temperature phase

The EISF calculated as in section 2 should not contain the Debye–Waller factor, and in any case an incomplete cancellation of this factor cannot produce the large temperature dependence of the experimental EISF. On the other hand, the theoretical EISF is calculated from a geometric model of rotations, which only takes into account the initial and final equivalent orientations of the molecule, and therefore is temperature independent. Consequently, the temperature dependence of the EISF must be attributed to the presence of more components in the scattering function. However, an additional Lorentzian did not improve the fits.

It should be noted that there can be a continuous transformation from the lower-bound to the upper-bound model by a decrease of the jump rates of rotations around the C_2' axes. C_2' jumps give rise to a Lorentzian component, λ_1, with a structure factor $(A_{A_2}+A_{B_1})$ lower than the structure factor, A_E, of the Lorentzian, λ_2, determined by the C_{2z} jumps (figure 4) in the Q range of our experiments. If the jump rate of C_2' rotations decreases with the temperature according to an Arrhenius law, the width of the Lorentzian with structure factor $A_{A_2} + A_{B_1}$ (expression (1)) will decrease, and this quasielastic component will progressively die out into the EISF. We think that the second Lorentzian could not be fitted probably because of its lower intensity and lower width, and thus the jump rates of each type of rotation that would take place (C_2' and C_{2z}) could not be obtained.

In contrast to unlimited jump diffusion, where there is no elastic component, the central part of the neutron spectrum of rotational jumps in molecules is dominated by the elastic component, which gives the EISF. This dominant component, convoluted with

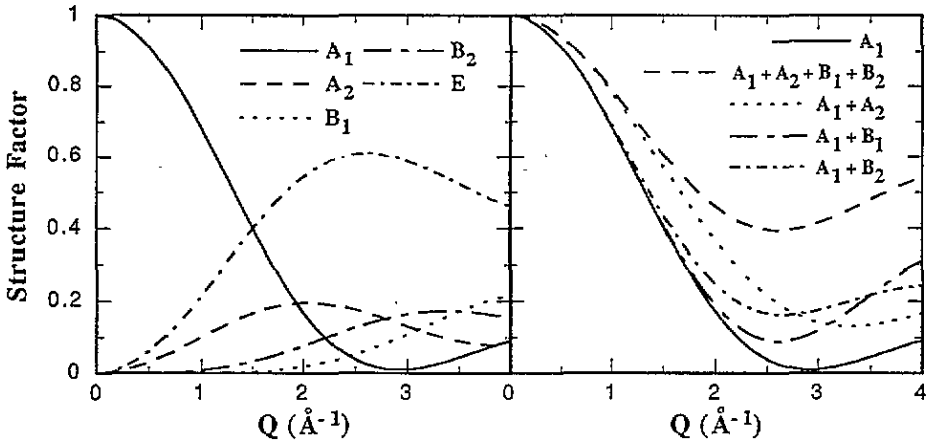

Figure 4. Structure factors of the scattering function for rotations about all the axes defined in figure 3. When rotations are restrained to the axes C_{2z} and C_2', the corresponding structure factors of the quasielastic components are $A_2 + B_1$ and E, and the EISF is $A_1 + B_2$.

the experimental resolution function, is easily fitted, as also happens with the long tails of the broad Lorentzian component, while the narrow Lorentzian component only contributes at the base of the elastic component (broadened by the resolution). This means that only a small energy range of the spectrum outside the resolution function will show a significant intensity originating from the narrow quasielastic component, and as a consequence the inflexion points of the corresponding convoluted Lorentzian function might be excluded from that region, avoiding the assignment of that intensity to a second Lorentzian function in the numerical fits. As an example of the quality of the fits with a delta function and a single Lorentzian function, a plot of a typical experimental spectrum and its corresponding fit is shown in figure 5(*a*).

The argument above proposes that the total spectrum actually contains two quasielastic components, and the intensity of the narrow one has been shared by a single Lorentzian function and the elastic component in the fits. The effect of fitting a single Lorentzian instead of two can be simulated analytically in the following way. We have assumed a triangular resolution function (this is a reasonable approximation for the TOF spectrometers used). The half widths of the two Lorentzian components are given by expression (1). The jump rate $\tau_{C_2'}^{-1}$ is assumed to be smaller than $\tau_{C_{2z}}^{-1}$, so the main jump process is 180° rotations around the C_{2z} axis, and the width of the broad Lorentzian (structure factor $A_E(Q)$) is dominated by this process. If each rotational process follows an Arrhenius law and we assume that the Lorentzian function used to fit the experimental spectra is essentially the broad component of the full model, the half widths of the two Lorentzian functions can be written

$$\lambda_1 = 2\gamma_0' e^{-E_a'/kT} \qquad \lambda_2 = \gamma_0 e^{-E_a/kT} + \gamma_0' e^{-E_a'/kT} \tag{2}$$

where E_a and γ_0 should be given by the value obtained from the fits with a single Lorentzian function, and would correspond to the C_{2z} jumps, while E_a' will be larger than E_a, and should correspond to a less efficient process. We shall also assume that the two prefactors are equal, $\gamma_0 = \gamma_0'$.

The scattering function (1) has been convoluted with the triangular resolution function in order to give a spectrum similar to those obtained from the spectrometer. The simulated

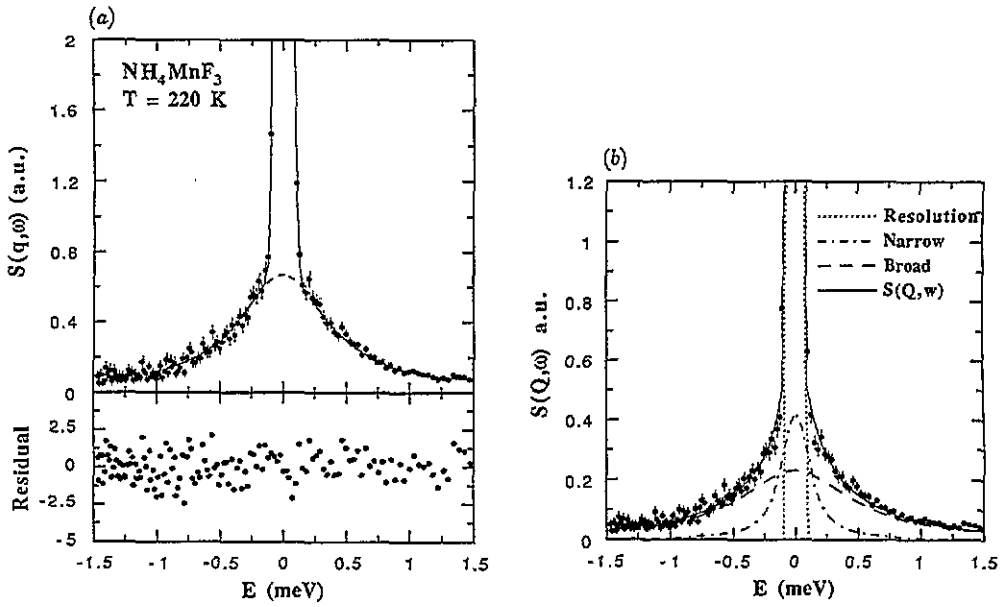

Figure 5. (*a*) The experimental quasielastic neutron scattering spectrum of NH_4MnF_3 at 220 K and momentum transfer $Q = 1.53$ Å^{-1}. The full line is the fit with a delta function and a Lorentzian function convoluted with the experimental resolution function. The broken line is the quasielastic component convoluted with the resolution function. (*b*) A simulated spectrum, convoluted with a triangular resolution function, as explained in the text: full line, total scattering function with a delta function and two Lorentzian functions; broken lines, broad and narrow quasielastic components; dotted line, resolution function; parameters of the calculation, $E_a = 62.9$ meV, $E_a' = 100$ meV, $Q = 1.5$ Å^{-1}.

EISF has been calculated as the addition of the elastic intensity of the model with only C_{2z} and C_2' rotations (structure factor $A_{A_1}(Q) + A_{B_2}(Q)$) and the area of the Lorentzian of width λ_1 that lies within the width of the resolution function, since this intensity would have been attached to the elastic component in the fits with a single Lorentzian function. This calculation has been done as a function of the temperature (λ_1 and λ_2 given by expression (2)), and using the values of γ_0 and E_a from the initial fits with a single Lorentzian function.

The results of these calculations can be seen in figure 6, where the EISF corrected for the resolution effect is shown for the compound NH_4MnF_3, in the high-temperature phase and the experiment with neutrons of incident wavelength 4.9 Å. A calculated spectrum, including the quasielastic components, is also shown in figure 5(*b*) to be compared to the experimental spectrum in figure 5(*a*). It can be seen that the simulated EISF varies between the two theoretical limits ('upper' and 'lower' limits) corresponding to only one (C_{2z} axis) and two (C_{2z} and C_2' axes) rotational processes. This variation reproduces the experimental EISF within the uncertainty of the experiment (the error bars have not been included in the figure for clarity, but they can be seen in figure 1(*d*)) for a value $E_a' \simeq 100$ meV, except for the largest value of the momentum transfer in that experiment, where multiple-scattering effects are not negligible.

A model that includes 120° jumps around threefold axes (C_3) of the tetrahedron, or the cube inscribing it, and in addition jumps around the three equivalent axes C_2 and the three equivalent axes C_2', gives the same EISF as the model with only C_2 and C_2' jumps. This is a consequence of the fact that the time independent distributions of sites yielded by the C_2

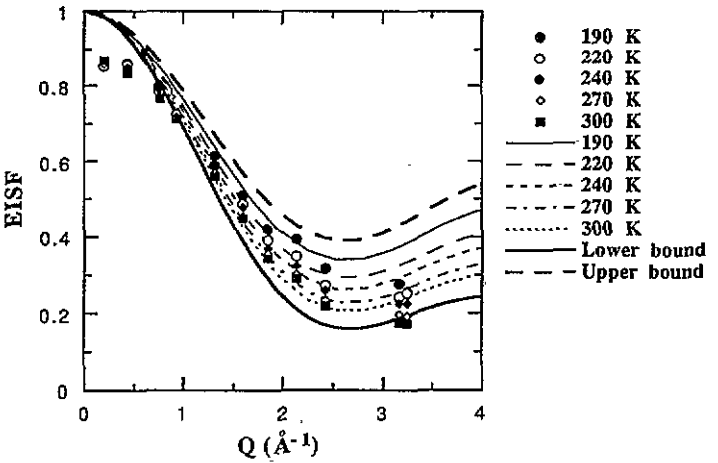

Figure 6. A simulation of the effect of the presence of a narrow quasielastic component fitted as elastic intensity on the EISF: points, experimental EISF; lines, simulated EISF as explained in the text; upper and lower bounds, C_{2z} jumps only and C_{2z} plus C_2' jumps, respectively.

jumps and the C_3 jumps are identical.

However, the addition of 120° jumps around molecular C_3 axes to the previous models (180° around C_2 and/or C_2' axes) would not allow for the change of the EISF with temperature. Indeed, the three C_3 symmetry axes of the tetrahedron are necessarily equivalent, so that the contribution of these 120° jumps to the EISF cannot be reduced to jumps on a single C_3 axis as temperature decreases, which would yield the same EISF as 180° jumps around a single C_2 axis. On the contrary, the absence of 120° jumps around C_3 axes leads to the D_4 point group for the rotations contributing to the EISF. This group allows for the non-equivalence of the C_2 axes, so that, as the transition temperature is reached, the permanence of only C_{2z} jumps (the axis z is determined by the orientation of the NH_4^+ tetrahedron in the crystal field) is consistent with the EISF at temperatures near the transition.

The existence of a preferential axis in the NH_4^+ perovskites is a consequence of the orientation of the NH_4^+ tetrahedron in the cubic perovskite lattice, and this particular orientation yields an effective symmetry D_{2d} for the molecule in the lattice, which is a point group isomorphous to D_4 (only proper rotations). It should be noted that the situation encountered in the NH_4^+ perovskites is different from that of NH_4Cl, where the effective symmetry is T_d (isomorphous to O), since all symmetry axes of the tetrahedron coincide with some symmetry axes of the crystal structure. Consequently, in NH_4Cl no preferential axis is determined by the orientation of the molecule.

The isotropic rotational diffusion also produces an EISF with more than one Lorentzian function (actually an infinite number of components), which may yield a temperature dependence of the experimental EISF due to instrumental resolution effects. However, this type of rotational motion is in conflict with the existence of well defined orientations observed by diffraction (Helmholdt *et al* 1980, Rubín *et al* 1994) and Raman spectroscopy (Bartolomé *et al* 1985, Agulló-Rueda *et al* 1988), and, therefore, this model will not be considered.

4.3. The model of rotation in the low-temperature phase

The experimental EISF corresponding to the compound NH_4MnF_3 in the low-temperature phase is even higher than that of only 180° rotations around a single twofold axis

(figure 7(*a*)). In order to explain such striking behaviour, a model is proposed where only two orientations of the NH_4^+ ion with different energies will be considered, and thus there is a difference of thermal population. At the transition temperature, the model should converge into the model of only 180° rotations around the C_{2z} axis of the high-temperature phase (the 'upper bound' of the models in this phase). Thus, the axis of rotation will be near the former twofold axis of the high-temperature phase (in the low-temperature structure the crystal has no twofold axis), and all H atoms will jump about the same distance. Therefore, in this model the jump process of every H atom is equivalent to the classical jumps of a single proton in an asymmetric double-well potential (figure 7(*b*)). In this model (Beé 1988)

$$S(\omega, Q) = A_1(Q)\delta(\omega) + [A_2(Q)/\pi]\lambda/(\omega^2 + \lambda^2)$$

$$A_1(Q) = [1/(1+\rho)^2][1 + \rho^2 + 2\rho j_0(Qd)]$$

$$A_2(Q) = [2\rho/(1+\rho)^2][1 - j_0(Qd)]$$

$$\lambda = (2/\tau_1)(1+\rho) \qquad \rho = \tau_1/\tau_2$$

where d is the jump distance and τ_1^{-1} and τ_2^{-1} are the jump rates from sites 1 and 2, respectively. In thermal equilibrium, ρ is related to the energy difference, Δ, through

$$\Delta = -k_B T \ln \rho.$$

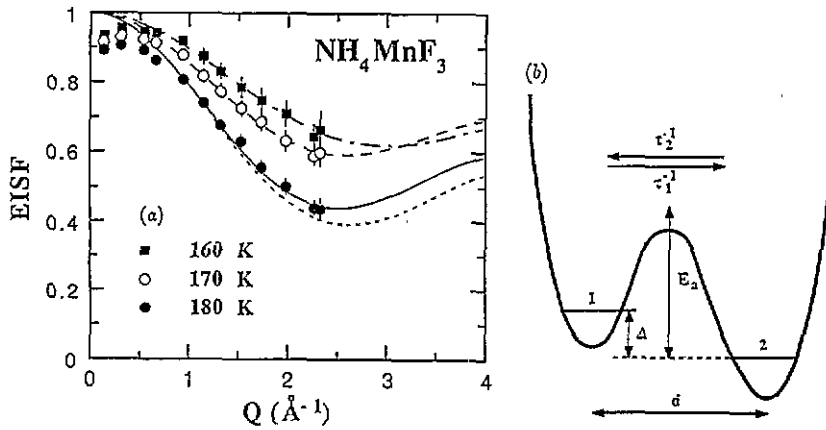

Figure 7. (*a*) The experimental EISF of NH_4MnF_3 below T_c (points), fitted EISF (——, two-site model, T = 180 K; – – –, two-site model, T = 170 K; — · —, two-site model, T = 160 K) and calculated EISF (·····, 180° rotations around the axis C_{2z} of the cubic phase). (*b*) The asymmetric double-well potential of the two-site model used to interpret the EISF in the low-temperature phase of NH_4MnF_3.

We fitted the experimental EISF of NH_4MnF_3 at 180, 170 and 160 K with d and ρ as fitting parameters in the expressions above. At 180 K we obtained Δ = 9 meV, while at 170 and 160 K the result was 19.4 meV. The jump distance varied from 1.8 Å at 180 K to 1.5 Å at 160 K. These jump distances are consistent with rotations about an axis near a twofold or threefold axis of a regular NH_4^+: d = 1.71 Å (an N–H distance of 1.05 Å

is assumed), while fourfold rotations would yield a jump distance of only 1.21 Å. The discrepancies can be attributed to distortions of the molecule, but only partially, since the jump distance at 160 K would correspond to an H–N–H angle of 91°, which is too small. Though we cannot propose a spatial description of the two orientations involved, it can be said that both orientations are related by a rotation of approximately 180° around the (undistorted NH_4^+) twofold axis C_{2z}.

5. Discussion

5.1. Models of rotation

5.1.1. The high-temperature phase. In the high-temperature cubic phase, the rotational jump with the largest rate is a 180° rotation about a fourfold crystal axis that is also a twofold NH_4^+ axis. This axis is determined by the orientation of the NH_4^+ tetrahedron in the cubic perovskite cage (figure 3). Thus the main rotational process leaves the NH_4^+ ion invariant. However, as argued above, other kinds of rotation may exist at high temperatures: 180° jumps about twofold crystal axes that are not rotator axes, which would give a change in the orientation of the molecule. This process has a smaller rate, and only the first kind of 180° rotation could be observed at the transition temperature. Therefore the NH_4^+ ions would freeze in a single orientation as the transition temperature is approached.

In the QNS work on NH_4ZnF_3 (Steenbergen *et al* 1979) several models were tried to explain the experimental EISF. The authors concluded that the most frequent jump of the NH_4^+ ion corresponded to 90° rotations around the (crystal) fourfold axis coincidental with an NH_4^+ twofold axis. In the light of our experimental results extended to NH_4MgF_3 and NH_4MnF_3, and the model that explains them, a revision of that work is necessary.

First, it is necessary to recall some aspects of the method they used to obtain the EISF. The EISF was obtained from the intermediate function, $I(Q,t)$, in the $t \to \infty$ limit. The intermediate function was obtained by the numerical Fourier transform of the experimental scattering spectrum. In the time space, the experimental intermediate function includes the resolution function as a multiplicative factor (in the energy space, scattering from the sample and resolution are convoluted), which was removed to obtain the intermediate function from the sample without resolution effects. This function must verify the limit condition $I(Q,\infty) = 1$ when $Q \to 0$, and in order to fulfill this condition the experimental values were normalized. This factor was said to include multiple-scattering corrections and uncertainties in the scattering function (e.g. background). However, in this way the multiple-scattering corrections were assumed to be Q independent. This probably overestimated that correction for intermediate scattering angles. Moreover, the method employed by Steenbergen and coworkers does not remove the Debye–Waller factor, which strongly depends on the momentum transfer. Finally, the EISF was obtained for temperatures between 200 and 273 K, while the transition temperature is 115 K.

In figure 8, the experimental EISF of Steenbergen *et al* (1979) has been plotted, after removing the normalization factor. After this *inverse* correction the EISF still contains the Debye–Waller factor. In the same plot the EISF calculated for the models proposed in section 4 have also been included. By inspection of figure 8, multiple-scattering effects are significant for low values of Q, in a much stronger way than in our experiment (a value $\mathrm{EISF}(Q \to 0) \simeq 0.72$ can be extrapolated).

Apparently, the experimental points at 200 K agree well with the model of 90° rotations around a single axis (curve s in figure 8), as proposed by Steenbergen. However, the EISF of the high values of Q must be strongly affected by the Debye–Waller factor, and the data

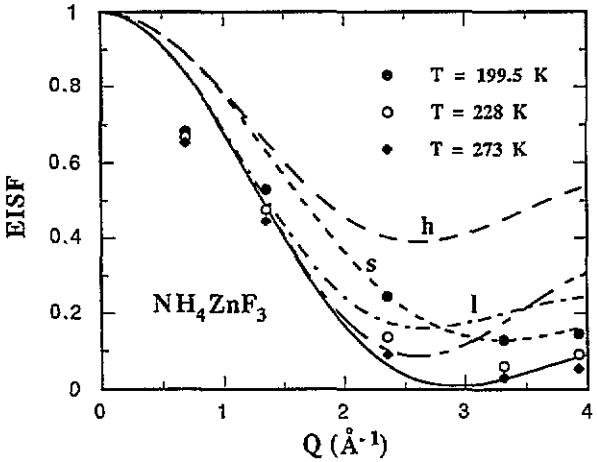

Figure 8. The experimental EISF of NH_4ZnF_3 obtained by Steenbergen *et al* (1979). The data have been transformed as explained in the text to enable comparison with those of figure 1 of the present work (the theoretical curves are the same as in figure 1).

corrected by this factor must lie between the limiting models proposed in subsection 4.1 (curves 1 and h). Moreover, this correction is larger with increasing temperature. On the other hand, the temperature dependence of the EISF in these measurments (performed at temperatures above 199 K, while $T_c = 115$ K) shows a tendency towards the model of curve h (180° rotations on a single axis). Thus, we may conclude that the model where only twofold rotations are the main process with a preferential axis (curve 1 in figure 8) gives the best agreement with the previous NH_4ZnF_3 experimental data, describing the Q dependence and temperature dependence.

At first sight, 180° rotations seem unphysical since they would involve jumps over high barriers. Moreover, 90° jumps around the same axis should be more probable than the 180°. In fact, 90° or 180° rotations around a fourfold axis, if the rotation is viewed as continuous rotations of a rigid body around a fixed axis, involve the highest potential barriers. However, it should not be forgotten that the actual jump path is not determined in the EISF modelling, but only the geometric relationship between the initial and final orientations. On the other hand, it is interesting to notice that 180° rotations around twofold NH_4^+ axes are equivalent to double rotations of 120° around threefold axes, which involve lower potential barriers ($V(3)/V(2) \simeq 0.5$†, where $V(n)$ is the potential barrier for n-fold jumps). In fact, the point group of proper rotations of a tetrahedron is isomorphous to a group with only single and double ternary rotations

$$T' = \{E, C_1^{\pm}, C_2^{\pm}, C_3^{\pm}, C_4^{\pm}, C_2^- C_1^+, C_3^- C_1^+, C_4^- C_1^+\}$$

where $C_i^{\pm}$ ($i = 1, 2, 3, 4$) are ternary rotations around the four threefold axes of the tetrahedron, and $\pm$ indicates the sense of rotation. This argument suggests the possibility of other paths for the jump process different from rotations around the C_{4z} axes. The importance of multiple jumps has already been shown for the NH_4^+ ion in NH_4Cl (Gerling and Hüller 1983).

† Calculated for typical values $\beta_4 = -0.25$, $\beta_6 = 0.97$ in the potential expansion $V(\omega) = \beta B(\beta_4 V_4(\omega) + \beta_6 V_6(\omega))$ in the cubic phase ($B = 8.48$ K is the rotational constant).

5.1.2. The low-temperature phase. In the low-temperature phase, the preferential orientation of the NH_4^+ ion is determined by the crystal structure (Laguna *et al* 1993), but a relaxation process can still be observed at temperatures below T_c. This process is not produced by orientational disorder in the same way as in the high-temperature phase (jumps between six equivalent orientations in the cubic structure). In the low-temperature phase there are two rotational states that correspond to similar orientations and different energies (about 19.4 meV difference), but the jump between them involves a rotation of about 180°. Therefore, the orientation of the NH_4^+ ion is essentially invariant in that phase.

For an energy difference of 19.4 meV, both rotational levels should be well populated at the temperatures where the measurements were carried out. The existence of an orientational disorder has also been suggested in our work with Raman spectroscopy (Laguna *et al* 1993), but no unambiguous answer could be given for its origin. In fact, in the Raman work another origin for disorder is also suggested: NH_4^+ ions at different sites located at the boundaries of domains of the crystal twinnings that usually appear in the distorted phases of the perovskites. Such a kind of disorder is temperature independent (assuming that there is no essential change of size in the twinning boundaries). Thus, the temperature dependence of the EISF indicates that orientational disorder exists. Notwithstanding, this does not exclude the simultaneous existence of site disorder, since, though it would give rise to two Lorentzians (two rotational process), one of the possible processes could be unobservable with the resolution of the present experiments.

5.2. Activation energies

The activation energies derived from the temperature dependence of the quasielastic broadening confirm the trend of their increase with the cell parameters in both structural phases of these compounds. This trend has suggested that repulsive interactions should be important in the members of the family with smaller cell parameters (Mg and Zn), while the very high activation energy of the Cd compound should be attributed to large attractive forces other than the electrostatic one of point charges (Palacios *et al* 1989). The activation energies in the low-temperature phase are always larger than those in the high-temperature phase. This is the expected behaviour, confirmed by the present results of NH_4MnF_3 and NH_4CdF_3.

The known trend of higher activation energies for larger cell size in the cubic phase seems to indicate that the electrostatic interaction as the dominant interaction may be ruled out. This conclusion is based on the assumption that the activation energy is mainly dependent on the potential barrier for rotations, V_0, which should decrease with the cell parameter. However, more parameters take part in the activation energy of the rotational process. In fact, the activation energy is

$$E_a = V_0 - E_0 + E_s$$

where E_0 is the energy of the rotational ground state and E_s is the rotational energy of the rotator at the saddle point of the potential surface. The latter has been estimated as the energy level for the potential energy expanded around the saddle point (Svare *et al* 1979), and usually has been taken equal to E_0. In any case E_s is a parameter difficult to estimate, which should have a value between E_0 and $3E_0$ (Svare 1977), and it is necessary to compare predicted and experimental activation energies.

All the quantities intervening in the activation energy are temperature independent, as long as the interaction potential is also temperature independent. In the classical

approximation and for small oscillations, the jump rate, ν, is related to the potential function as (Vineyard 1957)

$$\nu = \left(\prod_{i=1}^{N} \nu_i \Big/ \prod_{i=1}^{N-1} \nu_i' \right) \exp\{-V_0/kT\}$$

where ν is related to the quasielastic full width at half maximum, Γ, as $\nu = \Gamma/2\hbar$. ν_i are the frequencies of the vibrational modes of the crystal (including the diffusing atom) when the diffusing atom (or molecule) is in the equilibrium position), ν_i' are the corresponding frequencies when the diffusing atom is at the saddle point, and V_0 is the difference of potential energy between the saddle point and the equilibrium position.

When the previous expression is compared to the Arrhenius law, $\hbar/(\Gamma/2) = \tau = \tau_0 \exp\{E_a/kT\}$, the prefactor τ_0 is now

$$\tau_0 = \hbar \left(\prod_{i=1}^{N-1} \nu_i' \Big/ \prod_{i=1}^{N} \nu_i \right) \exp\{(E_s - E_0)/kT\}$$

which shows that τ_0 is actually temperature dependent. However, this dependence will be negligible as long as the difference $E_s - E_0 \ll kT$. Moreover, if we assume as a first approximation $\nu_i = \nu_i'$, then simply $\tau_0 = \hbar/E_0$.

Within the precision of our measurements, especially for those where a large temperature range has been explored, no temperature dependence of the prefactor τ_0 is detected. This shows that the value $E_s = E_0$ can be taken for the fluoroperovskites and therefore $E_a = V_0$. For the high-temperature phase, this implies that the electrostatic point charge model still predicts increasing activation energies with cell parameter, contrary to the experimental result. Moreover, the trend of increasing prefactor τ_0 with decreasing cell parameter (table 2) gives rise to decreasing ground state energies ($E_0 = \hbar/\tau_0$), in contradiction to the point charge model.

In contrast, for the low-temperature phase recent determinations of the structures of NH_4MnF_3 and NH_4CdF_3 (Le Bail *et al* 1990, Laguna *et al* 1993) show that some N–F distances are shorter than those in the cubic phase. Therefore the electrostatic model should be tested again with the new structures and a comparison must be made between the experimental activation energies for the rotational jump process and the calculated ones with the parameter $E_s = E_0$. This will be treated in paper II along with the librational energies, which will also be calculated.

Another interesting fact in the dependence of the quasielastic broadening with the temperature is the step in the widths at the transition temperature for all the compounds of the series (figure 2). This step is connected to the trend of the activation energies and prefactors. Both the activation energy and prefactors, $\hbar/\tau_0$, increase when the compounds undergo the transition from the cubic to the distorted phase. In the simplest model, $E_0 = \hbar/\tau_0$, where E_0 is the energy of the ground state rotational level. In the harmonic approximation $E_0 = E_L$, where E_L is the energy of the first rotational level, which can be measured. As will be shown in paper II, where E_L is measured, the above estimation of E_0 from τ_0 fails, but the general trend is fulfilled. Since the activation energy in the low-temperature phase of NH_4CdF_3 is probably overestimated, the presence of the step cannot be assured but it is likely to exist if an extrapolation of what occurs in the other compounds of the series is considered.

An Arrhenius law for the rotational process can be derived from the absolute rate theory (e.g. Vineyard 1957), in which the jump rate of a diffusion process is calculated

as the product of the occupation factor of an energy level above a saddle point of the interaction potential energy ($\exp\{-E_a/kT\}$) and a factor proportional to the rate of crossing along the saddle point to a new position or orientation. This last factor is what we have denoted prefactor $\hbar/\tau_0$. Thus, the increase in activation energy and prefactors when the fluoroperovskites undergo the phase transition to the low-symmetry phase indicate that the intensity of the interaction that constrains the angular displacements of the NH_4^+ group has increased and that the rate of crossing along the saddle point has also increased.

6. Conclusions

Quasielastic neutron scattering experiments carried out on the perovskites NH_4MF_3 (M=Mg, Zn, Mn, Cd) have provided information about the potential barriers for the rotational jump process and a spatial description of the rotations.

The experimental EISF has been analysed through several models for the geometry of the rotations between equilibrium orientations. In the cubic phase, the jumps with the largest jump rate are 180° rotations around an NH_4^+ twofold axis coincident with a fourfold crystal axis. This axis is determined by the orientation of the molecule in the perovskite structure. As temperature is lowered towards the transition temperature, only that kind of jump is observed in the experimental time range. The activation energies of the rotational process have been obtained, and range from 44.8 meV for NH_4MgF_3 to 128 meV for NH_4CdF_3, which clearly shows the trend of increasing activation energy with cell parameter, already known in the low-temprature phase by NMR studies. The temperature dependence of the EISF in the high-temperature phase of these compounds has been interpreted as an effect of the analysis procedure induced by the presence of a narrow quasielastic component that could not be fitted directly. Alternatively, this has been simulated analytically, estimating the activation energy of the second rotational process (180° jumps around the C_2' axes) to be $E_a' \simeq 100$ meV. The verification of this activation energy requires further experiments with a narrower resolution such that the narrow quasielastic component could be obtained neatly.

In the low-temperature phase, a single orientation of minimum energy exists, though a jump process can still be observed between a minimum-energy equilibrium orientation and another non-equivalent near orientation of energy about 19.4 meV higher.

Acknowledgments

The authors are indebted to H Büttner and A J Dianoux for assistance in the experiments and to the ILL for its hospitality. R Hempelmann is acknowledged for tunnelling tests and Professor S Altmann for fruitful discussions on symmetry. J Rubín acknowledges a grant from the Ministerio de Educación y Ciencia. This work has been supported by the CICYT project PB92-1077.

References

Agulló-Rueda F, Calleja J M and Bartolomé J 1988 *J. Phys. C: Solid State Phys.* **21** 1287
Agulló-Rueda F, Calleja J M and Tornero J D 1987 *Solid State Physics* vol 62 (New York: Academic) p 551
Bartolomé J, Navarro R, González D and de Jongh L J 1977 *Physica* B **92** 23

Bartolomé J, Palacio F, Calleja J M, Agulló-Rueda F, Cardona M and Migoni R 1985 *J. Phys. C: Solid State Phys.* **18** 6083
Bée M 1988 *Quasielastic Neutron Scattering* (Bristol: Hilger)
Blank H and Maier B 1988 *The Yellow Book: Guide to Neutron Research Facilities at the ILL* (Grenoble: Institut Laue-Langevin)
Bonori M and Terenzi M 1974 *Chem. Phys. Lett.* **27** 281
Brom H and Bartolomé J 1981 *Physica* B **111** 183
Burriel R, Bartolomé J, Navarro R and González D 1981 *Recent Developments in Condensed Matter Physics* vol 4, ed J T Devresse *et al* (New York: Plenum) p 1
Dahlborg U, Larsson K E and Pirkmajer E 1970 *Physica* **49** 1
Fayos J and Tornero J 1993 *Ferroelectr. Lett.* **16** 43
Gerling R W and Hüller A 1983 *J. Chem. Phys.* **78** 446
Ghosh R 1985 *ILL Internal Report*
Grimm H, Courtens E, Dorner B and Monkenbusch M 1989 *Physica* B **156 & 157** 192
Helmholdt R B, Wiegers G A and Bartolomé J 1980 *J. Phys. C: Solid State Phys.* **13** 5081
Hüller A and Press W 1978 *Inelastic Neutron Scattering 1977* vol 1 (Vienna: IAEA) p 231
Hüller A and Raich J 1979 *J. Chem. Phys.* **71** 3851
Kearley G J and Oxton I A 1983 *Advances in Infrared Spectroscopy* vol 10, ed R J H Clark and R E Hester (New York: Wiley) ch 2
Kim J, Goyal P S, Venkataraman G, Dasannacharya B A and Thaper C L 1970 *Solid State Commun.* **8** 889
Laguna M A, Sanjuán M L, Orera V M, Rubín J, Palacios E, Piqué M C, Bartolomé J, Berar J F and Leblanc M 1993 *J. Phys.: Condens. Matter* **5** 283
Le Bail A, Fourquet J L, Rubín J, Palacios E and Bartolomé J 1990 *Physica* B **162** 231
Leung P S, Rush J J and Taylor T L 1972 *J. Chem. Phys.* **57** 175
Livingston R C, Rowe J M and Rush J J 1974 *J. Phys. Chem.* **60** 4541
Lucazeau G, Chahid A, Boquet J F, Dianoux A J and Roberts M P 1990 *Physica* B **164** 313
Palacios E, Bartolomé J, Burriel R and Brom H 1989 *J. Phys.: Condens. Matter* **1** 1119
Palacios E, Bartolomé J, Navarro R, García J, González D and Brom H B 1984 *Ferroelectrics* **55** 187
Palacios E, Navarro R, Burriel R, Bartolomé J and González D 1986 *J. Chem. Therm.* **18** 1089
Piqué C, Palacios E, Burriel R, Rubín J, González D, Navarro R and Bartolomé J 1990 *Ferroelectrics* **109** 27
Prager M, Press W, Alefeld B and Hüller A 1977 *J. Chem. Phys.* **67** 5126
Raaen A M, Svare I and Fibich M 1982 *Phys. Scr.* **25** 957
Rubín J, Bartolomé J, Magerl A, Visser D, Kearley G J and de Graaf L A 1989 *Physica* B **156 & 157** 353
Rubín J, Palacios E, Bartolomé J and Rodriguez-Carvajal J 1994 *J. Phys.: Condens. Matter* submitted
Steenbergen Chr, de Graaf L A, Bevaart L, Bartolomé J and de Jongh L J 1979 *J. Chem. Phys.* **70** 1450
Svare I 1977 *J. Phys. C: Solid State Phys.* **10** 4137
Svare I, Raaen A M and Thorkildsen G 1978 *J. Phys. C: Solid State Phys.* **11** 4069
Svare I, Thorkildsen G and Otnes K 1979 *J. Phys. C: Solid State Phys.* **12** 2177
Thibaudier C and Volino F 1973 *Mol. Phys.* **26** 1281
—— 1975 *Mol. Phys.* **30** 1159
Töpler J, Richter D R and Springer T 1978 *J. Chem. Phys.* **69** 3170
Vineyard G H 1957 *J. Phys. Chem. Solids* **3** 121
Woessner D E and Snowdon B J 1967 *J. Phys. Chem.* **71** 952